Discoloration of Aqueous Methylene Blue Using Bimetallic Fe-Cu NPs in Comparison with Fe NPs

T. Shahwan[1*], M. Anjass[2,3], R. Naser[1]

[1]*Chemistry Department, Birzeit University, Ramallah, West Bank, Palestine*
[2]*Institute of Inorganic Chemistry I, Ulm University, Albert-Einstein-Allee 11, 89081 Ulm, Germany*
[3]*Helmholtz Institute Ulm (HIU), Helmholtzstr. 11, 89081 Ulm, Germany*

Abstract

Fe nanoparticles and Fe-Cu bimetallic nanoparticles were synthesized, characterized, and comparatively tested for the discoloration of aqueous methylene blue (MB) dye. The materials were characterized using XPS, XRD, SEM, TEM, and Raman Spectroscopy. The nanoparticle materials showed chain-like morphology, with the particle size of Fe NPs being larger than that of Fe-Cu NPs. The dye removal studies included the effects of concentration, nanoparticle dose, temperature, and pH. The nanomaterials were also tried as heterogeneous Fenton catalysts. According to the results, the extent of MB removal by Fe NPs is larger than that of Fe-Cu NPs, and increases slightly with increasing the solution pH. Preliminary experiments showed that the removal capability of Fe-Cu NPs is significantly enhanced when used as heterogeneous Fenton catalysts.

1. Introduction

During the last two decades, intensive research has been conducted about the application of Fe nanoparticles (Fe NPs) in the abatement of various types of aqueous pollutants, and promising results have been reported [e.g. 1-5]. Nevertheless, one of the major difficulties associated with Fe NPs application is their tendency to aggregate, both during synthesis and in aqueous media. The size of Fe NPs aggregates in aqueous media can amount to tens of micrometers [6]. This aggregation largely limits the distance they can travel when injected in water bodies for in-situ treatment applications [7]. Among other factors, this has motivated the research about bimetallic nanoparticles, in which Fe is combined with other transition metals, in an attempt to enhance the performance of Fe NPs. So far, various bimetallic Fe nanostructures has been synthesized and used for water remediation purposes. Those include Fe-Au, Fe-Pd, Fe-Pt, Fe-Ag, Fe-Ni, Fe-Co, Fe-Cu and Fe-Al, which were produced using different chemical techniques, and the synergistic effects of the metals in these materials has been reported to convey effective removal of heavy metals and non-biodegradable organic pollutants [8-12].

In this study, Fe NPs and Fe-Cu bimetallic NPs were synthesized and tested for the removal of methylene blue (MB), which is a cationic dye and a medication, with the formula $C_{16}H_{18}ClN_3S$ (Scheme 1).
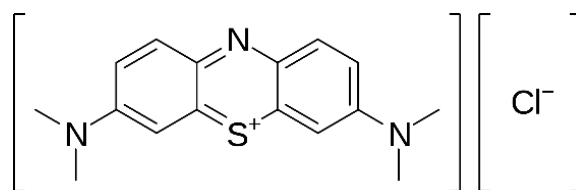
Scheme 1: Structural formula of methylene blue

The element Cu belongs to the same transition metal period of Fe in the periodic table, and its half-cell electrochemical reaction (Cu^{2+}/Cu) has a more positive standard electrode potential than that of Fe^{2+}/Fe. Thus, it is expected that the incorporation of Cu in the nanostructure of Fe will enhance the oxidation of elemental Fe into iron oxides, and consequently affect the electronic transfer cycle of Fe^{2+} ions. Fe-Cu bimetallic nanomaterials have been used in the catalytic degradation of various types of organic pollutants. The efficiency of Fe-Cu bimetallic nanoparticles was reported to depend on the density of Cu atoms on Fe surface in the catalytic removal of aqueous nitrobenzene. Small amounts of Cu on Fe surface could enhance the reduction, while a dense Cu layer could seriously decrease surface reactivity of the bimetallic nanoparticles [13]. In another study, it has been found that Cu^{2+} ions can enhance the degradation of trichloroethylene by Fe nanoparticles. The basic mechanism is of an electrochemical nature in which Cu^{2+} ions are reduced by Fe^0, as a result Cu^0 is deposited on the surface of the Fe nanoparticles while the produced Fe^{2+} ions enter the Fenton cycle [14].

Effective removal of MB by iron nanomaterials has been documented in literature in several studies [e.g. 15-18]. Recently, Fe-Cu bimetallic oxide were reported to be effective in the removal of MB using heterogeneous Fenton-like method [12]. However, our literature review did not yield studies about MB removal by Fe-Cu NPs in comparison with its removal using Fe NPs.

In this work, the nanoparticles were synthesized by the liquid phase reduction method. The materials were characterized using XPS, XRD, SEM-EDX, TEM, and Raman Spectroscopy techniques. The study tested the removal of MB by both types of nanoparticles under various reaction conditions such as concentration, nanoparticle dose, and pH. The materials were also tested as heterogeneous Fenton catalysts.

2. Material and Methods

2.1 Preparation of Nanoparticles

The nanoparticle samples were prepared using liquid phase reduction method, with sodium borohydride as the reducing agent, in accordance with procedures reported in previous publications [e.g. 18-20]. In order to prepare Fe NPs, 5.34 g (26.8 mmol) of $FeCl_2.4H_2O$ was dissolved in 25.0 mL ethanol-water solution (4:1 v/v). The solution was kept under magnetic stirring for 15 minutes at room temperature. In a separate beaker, 2.54 g $NaBH_4$ powder (67.2 mmol) was dissolved in 70.0 mL of water. The borohydride solution was then added to the iron solution using a burette, under continuous magnetic stirring of the mixture. The appearance of a black precipitate marked the formation of Fe NPs, during which H_2 gas evolution was observed. After the addition of the borohydride solution, the mixture was kept under stirring for another 15 minutes, and the formed Fe NPs were separated using vacuum filtration. The resulting Fe NPs powder was washed three times with absolute ethanol, and dried at 90oC for 6 h.

Fe-Cu NPs were prepared at Fe:Cu elemental mole ratio of 1:1. For this purpose, 4.25 g of $CuCl_2.2H_2O$ (25.0 mmol) and 4.97 g of $FeCl_2.4H_2O$ (25.0 mmol) were dissolved in 100 ml ethanol-water mixture (4:1 v/v), and was kept under continuous stirring for 15 min. $NaBH_4$ solution was prepared separately

by dissolving 3.79 g of $NaBH_4$ powder (100 mmol) in 70.0 mL water. The remaining steps were performed as above.

2.2 Characterization of Nanoparticle Materials

The samples were characterized using XRD, SEM-EDX, TEM, XPS and Raman Spectroscopy. Powder X-Ray Diffraction (XRD) patterns of the nanoparticles were recorded using a STOE Stadi P diffractometer, equipped with a Cu Kα (1.5405 Å) source, at 40 kV/ 40 mA. The samples were scanned in the 2θ range 10-80 degree.

X-ray Photoelectron Spectroscopy (XPS) spectra were acquired for the nanoparticle samples using a PHI 5800 MultiTechnique ESCA system. The source consisted of monochromatized Al-Kα (1486.6 eV) radiation, at take-off angle of 45°. The pass energies at the analyzer were 29.35 eV for detail scans, and 93.90 eV for survey scans.

Scanning Electron Microscopy (SEM) images and EDX mapping analysis of the nanoparticle materials were recorded using a Hitachi, S-5200 field-emission scanning electron microscope. The accelerating voltage is 10 kV, and the images were taken with the secondary electron detector.

The Transmission Electron Microscopy (TEM) images of the samples were recorded with a Jeol-1400 instrument. The accelerating voltage was 120 kV. After preparation, the samples were placed on a copper grid and fixed on the device holder, and the parameters were adjusted to obtain clear images. Raman spectra were collected with a Renishaw inVia microscope, using a 532 nm laser excitation.

2.3 Sorption Experiments

The effect of sorbent amount was studied at nanoparticle amounts of 10.0, 50.0 and 100.0 mg. In each experiment 25.0 ml of 100 mg L^{-1} dye solution was mixed with the nanoparticle sample and was kept in contact for 1 hour. The liquid solution was then separated from the solid material and the dye concentration was determined.

The effect of initial concentration of MB was studied at concentrations of 10, 50, 80 and 100 mg L^{-1}. In each sample, 50 mg of the nanoparticle materials was added to 25.0 mL of the dye solution, mixed and kept in contact for 1 h.

The effect of pH was studied at the initial pH values of 3.0, 5.0, 7.0 and 9.0. For this purpose, 50.0 mg of the nanomaterials was added to 25.0 ml of 100 mg L^{-1} MB solution, and mixed for 1 h.

The effect of temperature was studied by mixing 50.0 mg of the nanoparticle materials with 25.0 ml portion of the dye solution, at two initial concentrations of 80 and 100 mg/L. The mixture components were kept in contact for 1 h, at the temperatures of 298 K and 323 K.

In the heterogeneous Fenton experiments 50.0 mg of the nanomaterials was added to 25.0 ml of 100 mg L^{-1} MO solution, containing 2.5 ml 10% H_2O_2, and mixed for 1 h.

## 3. Results and discussion

3.1 Characterization of Nanomaterials

The XRD patterns of Fe and Fe-Cu NPs are shown in Fig. 1. Metallic Fe NPs are characterized by the most intense reflection (110) at 2θ value of 44.9° (Fig. 1a). The XRD pattern of Fe-Cu NPs is shown in Fig. 1b. The figure shows the diffraction signals of metallic Fe (110) and metallic Cu (111) and (200), in addition to the cuprite (Cu_2O) diffraction signals; (111), (200) and (220).

Typical TEM images of Fe and Fe-Cu NPs are given in Fig. 2. In general, the morphology of both nanomaterials is chain-like, and aggregation is dominant, a behavior which is attributed to the magnetic

attractive forces between the individual nanoparticles. The diameter of individual Fe NPs (Fig. 2a) is in the range 40-80 nm, and the dark color in the TEM image is attributed to the presence of metallic core of the nanoparticles, while the lighter one refers to metal oxides and/or oxohydroxides, usually constituting the shell part of the nanoparticles. As exhibited by Figs. 2b, the diameter of the individual Fe-Cu NPs appears to be approximately 10-30 nm.


(a)

(b)
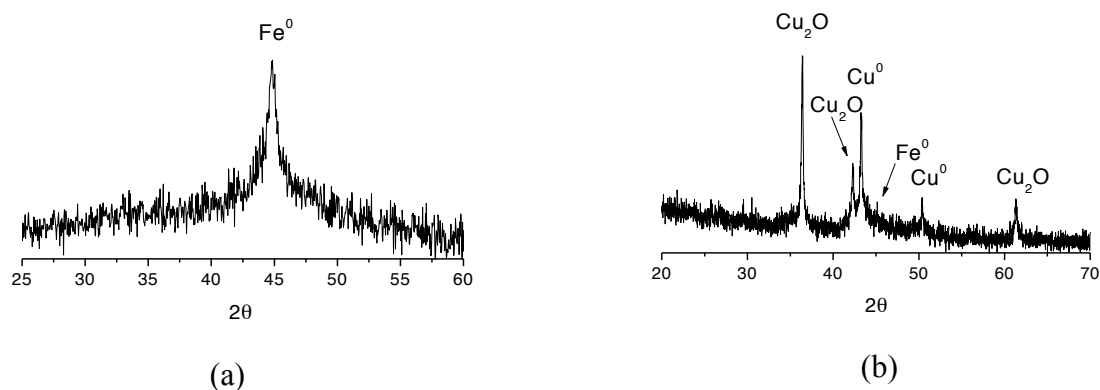
Figure 1. XRD diagrams of (a) Fe NPs, (b) Fe-Cu.

(a)

(b)
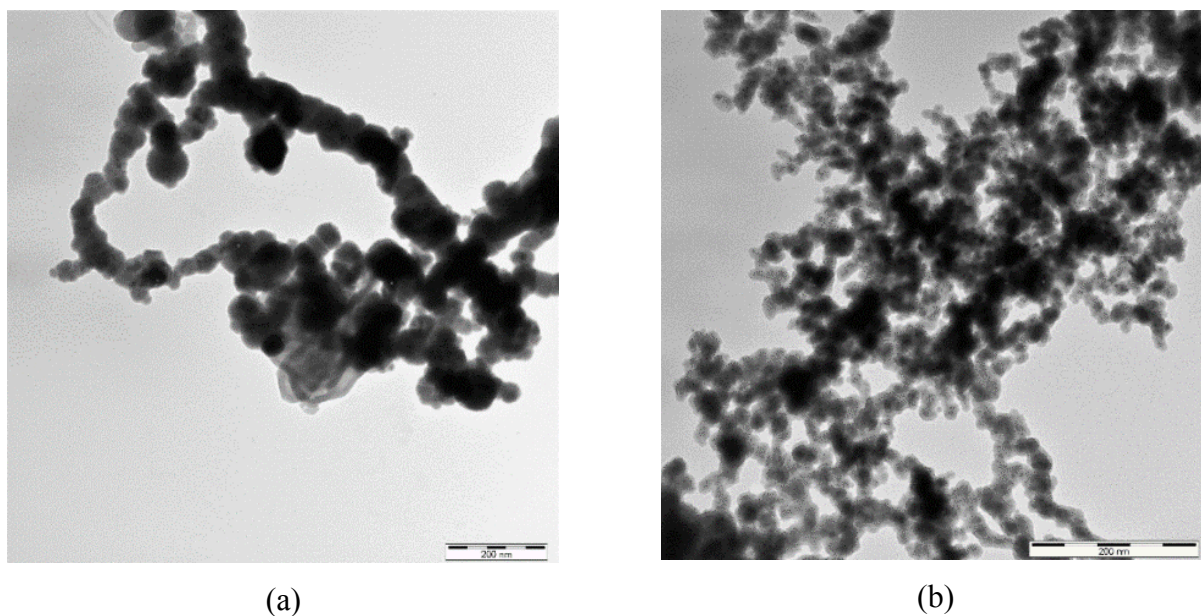
Figure 2. TEM images of: (a) Fe NPs, (b) Fe-Cu.

SEM-EDX elemental mapping images of the nanoparticle samples are shown in Fig. 3. Elemental mapping of Fe and O in Fe NPs is shown in Fig.3a, while Fig. 3b shows the elemental mapping of Fe-Cu NPs. The mapping images indicate a homogeneous distribution of the metals throughout the samples, and no distinct localization of pure Fe or Cu regions is observed. In all cases, the O signal is attributed to a metal oxide layer on the surface of the nanoparticles.

(a)

(b)
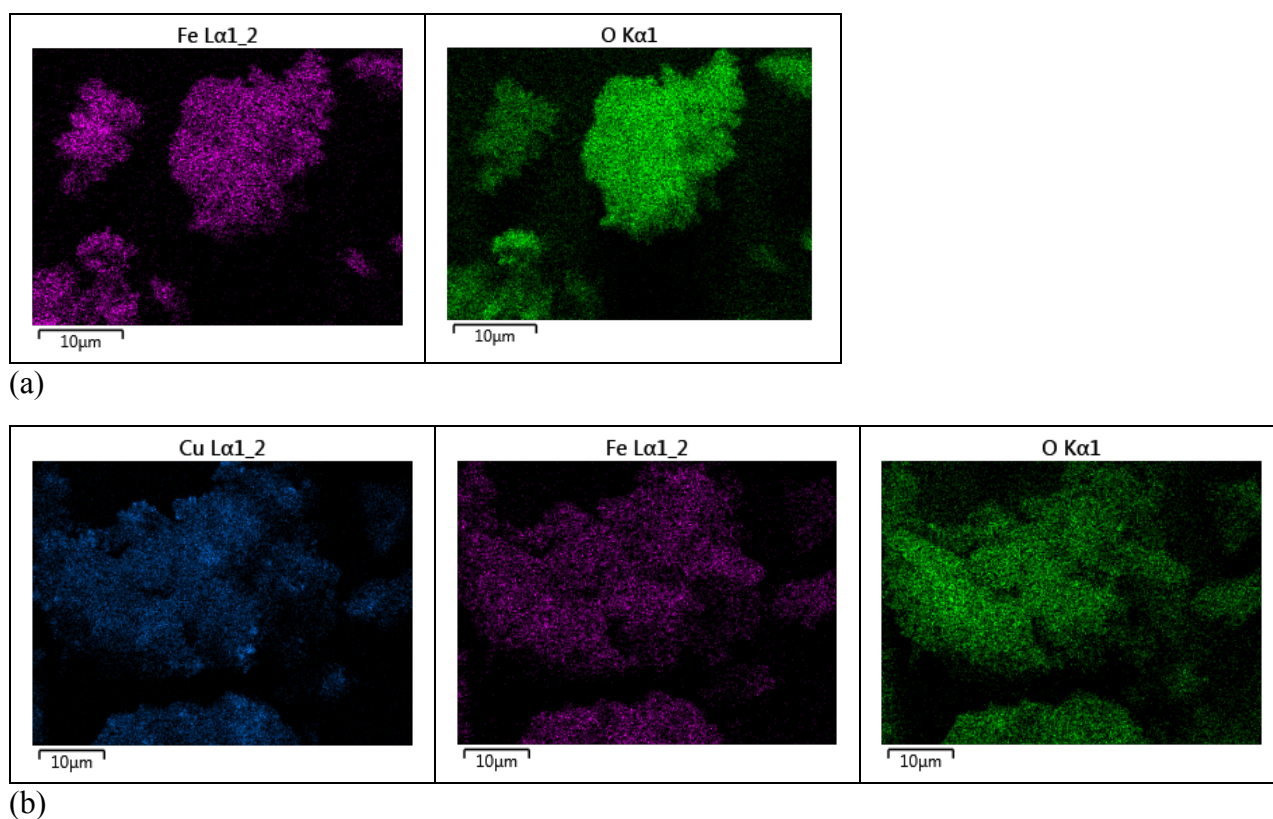
Figure 3. EDX elemental maps obtained for: (a) Fe NPs, (b) Fe-Cu NPs.

The nanoparticle samples were characterized using Raman Spectroscopy, as given in Fig. 4. The spectrum of Fe NPs (Fig. 4a) looks identical to that of a freshly prepared nZVI sample reported in literature [21]. The bands are similar to those reported for hematite in RRUFF database, [22], and -as such- are attributed to the shell part of Fe NPs. Fig. 4b shows the Raman spectrum of Fe-Cu NPs. Compared with the spectrum of Fe NPs, the bands in this spectrum appear to be blue shifted, and a new band is observed at 164 cm^{-1}. The bands in the spectrum did not match with those of cuprite or hematite, and might be characteristic for the bimetallic structure. Our literature review did not yield Raman spectra for Fe-Cu NPs, which can be used for comparison.
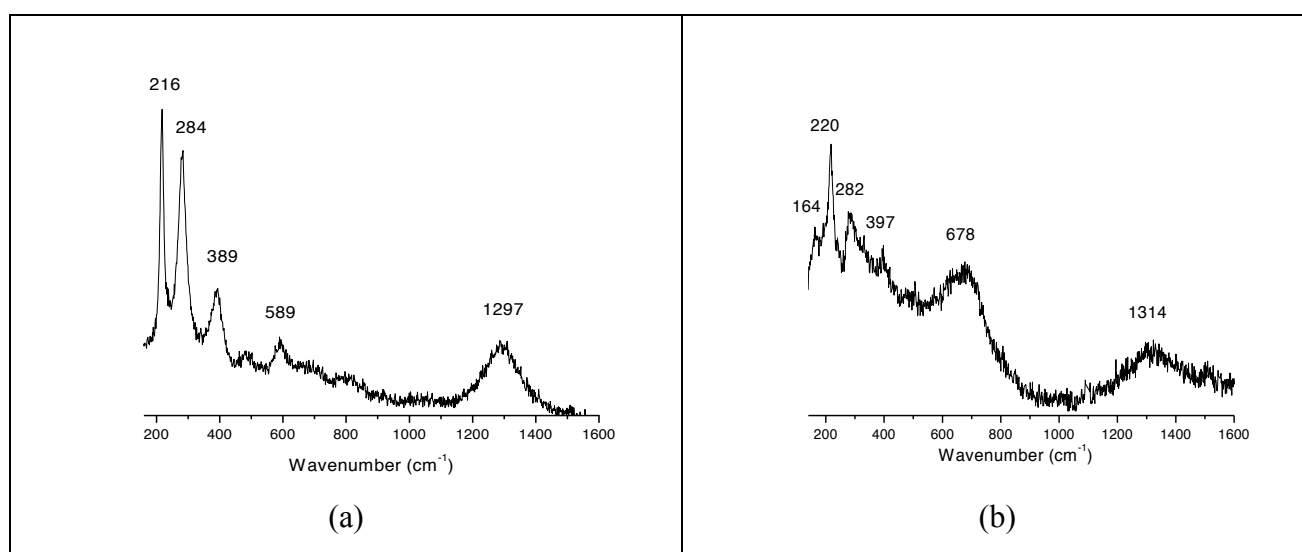
Figure 4. Raman spectra of: (a) Fe NPs, (b) Fe-Cu NPs.

The nanoparticle samples were also analyzed using XPS. The XPS survey spectra for Fe NPs and Fe-Cu NPs are shown in Fig. 5. The spectra display the elemental contents of the samples. In each case, the Na signal originates from the $NaBH_4$ used as a reducing agent during the synthesis, while the Cl signal is attributed to the iron chloride precursor. The C 1s peak arises from adventitious sources of carbon, while the O 1s feature originates mainly from O^{2-} in metal oxides of the nanoparticles shells. The Fe 2p features in Fe nanoparticles are shown in Fig. 6a. The features around 711 eV and 724 eV with difference of 13 eV are attributed to the binding energies of Fe^{2+} $2p_{3/2}$ and Fe^{2+} $2p_{1/2}$, respectively. While the features around 713 eV and 726 eV are attributed to the binding energies of Fe^{3+} $2p_{3/2}$ and Fe^{3+} $2p_{1/2}$, respectively.
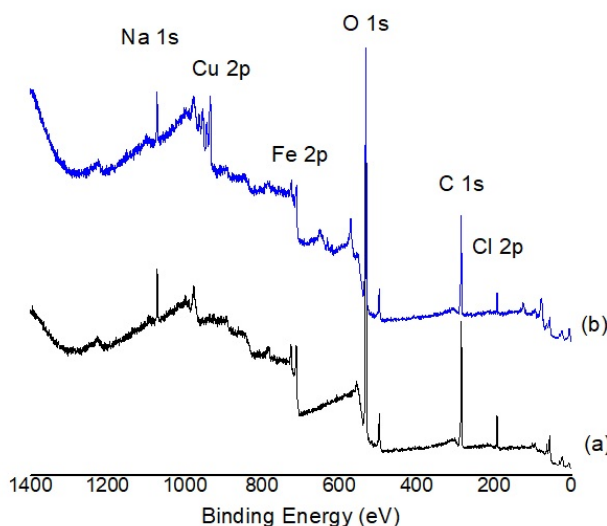

Figure 5. Wide XPS surveys of: (a) Fe NPs, (b) Fe-Cu NPs.

Fig. 6b shows the XPS of Fe 2p in Fe-Cu NPs. The features around 711 eV and 724 eV with difference of 13 eV are attributed to the binding energies of Fe^{2+} $2p_{3/2}$ and Fe^{2+} $2p_{1/2}$, respectively. While the features around 713 eV and 726 eV are attributed to the binding energies of Fe^{3+} $2p_{3/2}$ and Fe^{3+} $2p_{1/2}$, respectively. The peaks show slight binding energy shifts, which originate from the changes in the chemical environment of Fe in the two nanoparticle types. In general, the Fe 2p features form spectral envelopes of Fe(II) and Fe(III) signals are attributed to the iron oxides and iron oxyhydroxides, [23], which constitute the shell of Fe NPs. For both type of nanoparticles, the weak peak centered around 707 eV arises from Fe $2p_{3/2}$ of zero-valent iron (Fe^0), which forms the core of the nanoparticles.

The XPS doublet of Cu 2p in Fe-Cu NPs is shown in Fig.6c. Each of Cu $2p_{3/2}$ and Cu $2p_{1/2}$ show clear splits, suggesting that copper ions have at least two different chemical environments. The peaks at 932.2 and 951.9 eV with a difference of 19.7 eV, can be assigned to Cu $2p_{3/2}$ and Cu $2p_{1/2}$ peaks of zero-valent copper, Cu^0, or Cu(I) in Cu_2O. Meanwhile, the peaks at 934.6 and 954.5 eV, corresponding to the Cu $2p_{3/2}$ and Cu $2p_{1/2}$, can be attributed to the presence of Cu_2O or $Cu(OH)_2$ in the sample. The presence of Cu(II) is also verified by the distinct shake up satellite peaks in the spectrum [24].

3.2. Dye Removal Experiments

The two types of nanoparticles were comparatively tested for the removal of MB. The experiments investigated the effects of nanoparticle amount, initial MB concentration, temperature, pH, in addition to using the nanoparticle materials as heterogeneous Fenton catalysts. The results are presented and discussed in the following subsections.
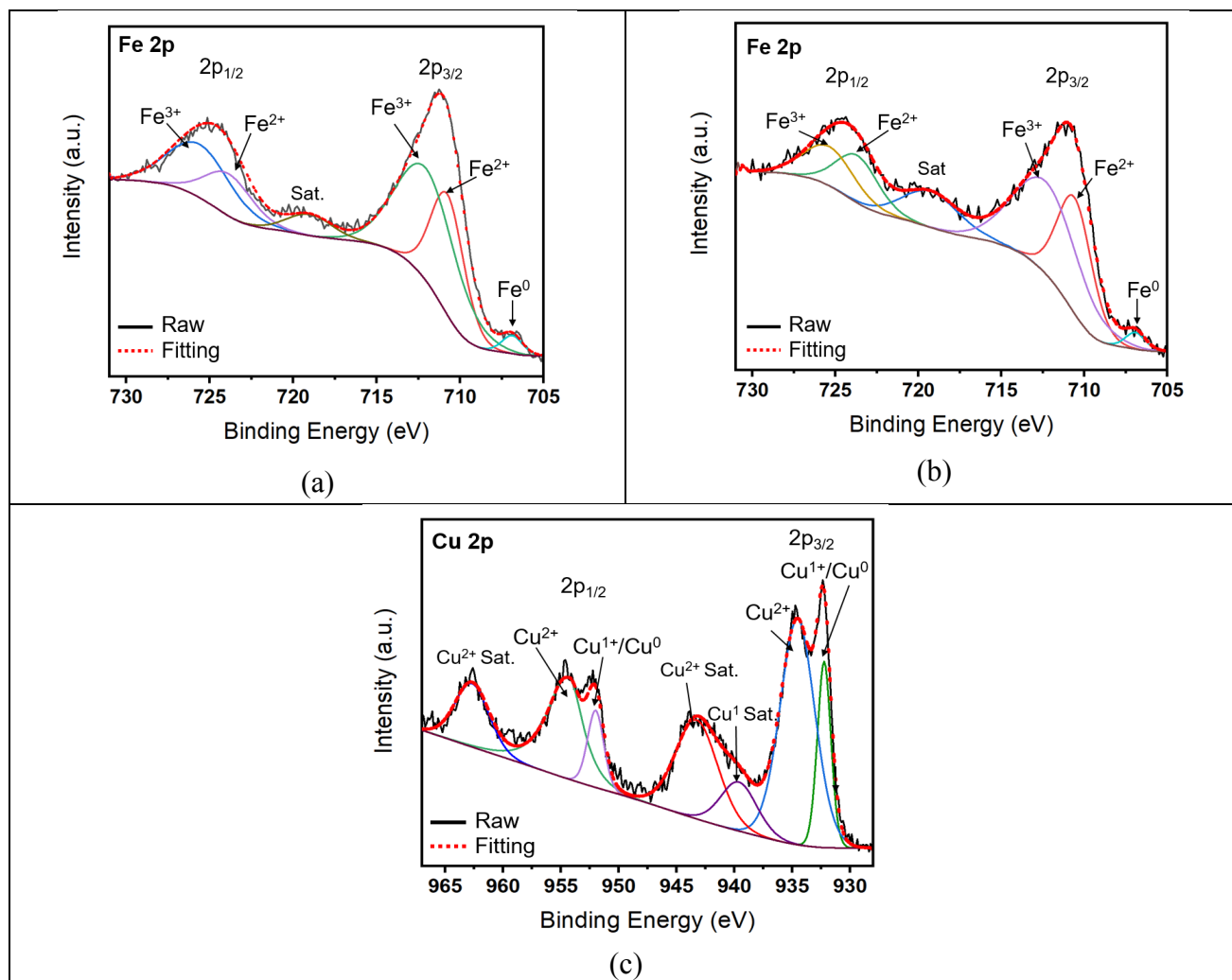
Figure 6. XPS spectra of: (a) Fe 2p in Fe NPs, (b) Fe 2p in Fe-Cu NPs, and (c) Cu 2p in Fe-Cu NPs.

3.2.1 Effect of nanoparticle amount

The results of these experiments reveal a gradual increase in the percentage removal of MB with the increase in the nanoparticle amount. The values of MB removal using Fe NPs were 86%, 95%, 97% at the NP doses of 10.0, 50.0, 100.0 mg, respectively. The corresponding amounts for MB removal using Fe-Cu NPs were 83%, 88%, 98%. This can be explained by the increase in the surface active sites with increasing the nanoparticle amounts. There seems a better performance for Fe NPs at 10.0 and 50.0 mg of NP amounts, however, the dye removal by Fe NPs and Fe-Cu NPs at the NP amount of 100.0 mg looks comparable, and the removal approaches completion in both cases. Based on the results of this experiment, the subsequent experiments were performed at 50.0 mg amounts of the nanoparticles.

3.2.2 Effect of initial concentration

The effect of initial dye concentration was studied using both types of nanoparticle materials. The obtained results are shown in Table 1. The relatively lower removal capacities of Fe-Cu NPs could be implying that copper oxides on the nanoparticle surfaces have less sorption capacity toward the dyes than iron oxides. In addition, the standard reduction potential of Cu^{2+}/Cu (0.34 V) clearly exceeds that of Fe^{2+}/Fe (-0.44 V), and thus in any redox mechanism involving dye degradation, Cu^{2+} ions could compete with dye molecules for the incoming electrons from the zero-valent core of the nanoparticles. Nevertheless, more investigation is needed to verify these conclusions.

Table 1: The values of MB concentrations in the solution (C, mg/L) and on the nanoparticles (Q, mg/g) at different initial concentrations.

C₀ (mg/L)	Fe NPs			Fe-Cu NPs		
	C (mg/L)	Q (mg/g)	% Removal	C (mg/L)	Q (mg/g)	% Removal
10.0	1.05	4.5	89.5	1.5	4.3	85.0
50.0	2.7	23.7	94.6	6.4	21.8	87.2
80.0	4.0	38.0	95.0	13.6	33.2	83.0
100.0	2.09	49.0	97.9	16.5	41.8	83.5

The obtained data was tested using Freundlich, Temkin, and Langmuir isotherm models. Langmuir isotherm can be linearized in four different form, and all of them were tested. The isotherm equations and the corresponding linear regression results are given in Table 2. None of the isotherms seems to provide adequate correlation with the data of MB on Fe NPs under the studied conditions. For Fe-Cu NPs, Freundlich isotherm demonstrated the best correlation with the sorption data on both nanomaterials. The linear plots of Freundlich isotherm can be seen in Fig. 7, for the sake of illustration. Although one of the four linear forms of Langmuir isotherm has a high coefficient of determination (R^2), the coefficients of the other three forms are poor, and as such, it is concluded that this model is not suitable for describing the experimental data. This result shows the need to check the linear correlation of the various linear forms of Langmuir isotherm, something rarely done in literature. The Temkin isotherm showed better correlation than Langmuir for Fe-Cu case, but its R^2 values were below those of Freundlich isotherm for both removal cases.

Table 2: The isotherm equations used in the linear fits and the corresponding R^2 values obtained from the removal of MB by both of nanoparticle types.

| Isotherm	Linear Equation	R^2 (Fe NPs)	R^2 (Fe-Cu NPs)
Freundlich	$lnQ_e = lnk + nlnC_e$; Plot lnQ_e vs lnC_e	0.6638	0.9830
Temkin	$Q_e = \frac{RT}{b}lnK_T + \frac{RT}{b}lnC_e$; Plot Q_e vs lnC_e	0.4613	0.9682
Langmuir	$\frac{C_e}{Q_e} = \frac{1}{KQ_m} + \frac{C_e}{Q_m}$; Plot C_e/Q_e vs C_e	0.9194	0.4475
	$\frac{1}{Q_e} = \frac{1}{KQ_m}(\frac{1}{C_e}) + \frac{1}{Q_m}$; Plot $1/Q_e$ vs $1/C_e$	0.8872	0.9965
	$Q_e = Q_m - \frac{1}{K}(\frac{Q_e}{C_e})$; Plot Q_e vs Q_e/C_e	0.7292	0.2267
	$\frac{Q_e}{C} = KQ_m - KQ_e$; Plot Q_e/C_e vs Q_e	0.7292	0.2267

(a)

(b)
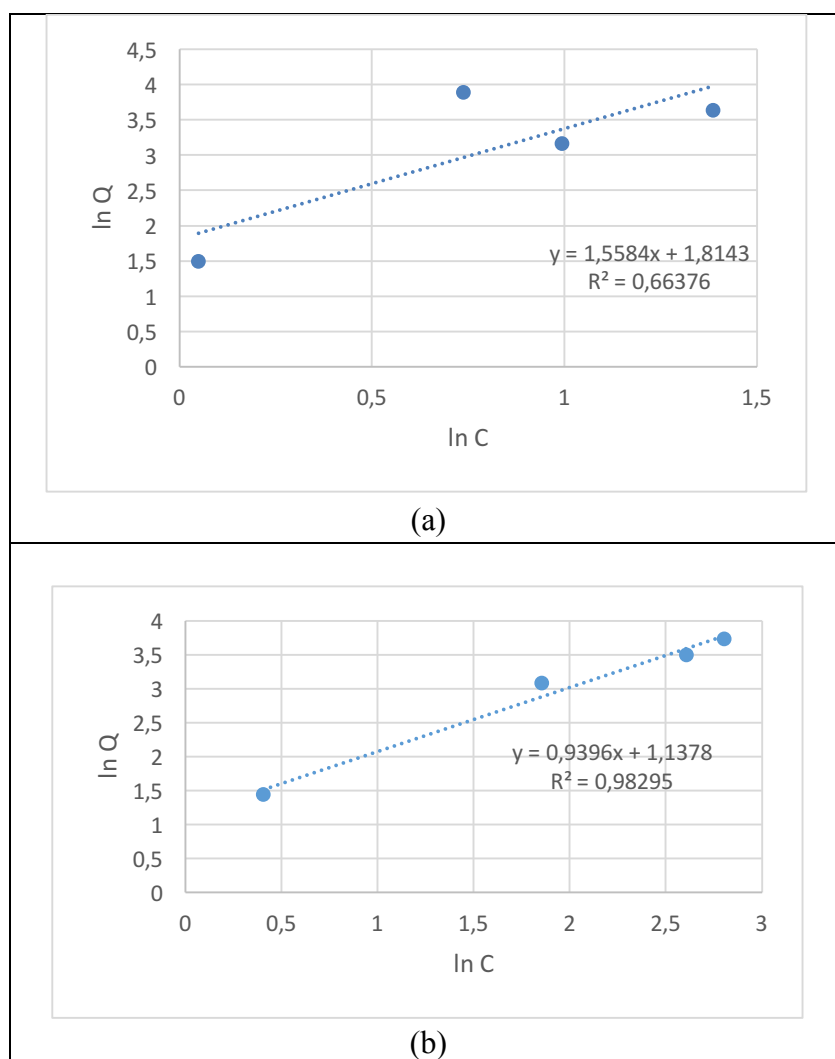
Figure 7. Freundlich isotherm fits for MB removal by: (a) Fe NPs, and (b) Fe-Cu NPs.

3.2.3 Effect of pH

The results of the experiments are shown in Fig. 8. The trend appears to be similar in the cases of Fe NPs and Fe-Cu NPs, where the percent removal of MB increases with increasing initial pH values from 3.0 to 5.0, and afterward small changes occur throughout the studied pH range. On the overall, the removal of MB by Fe NPs is higher than its removal by Fe-Cu NPs.

In aqueous media, methylene blue exists as hydrated MB^+, As the pH increases, the competition of H^+ decreases, and the surface sites become more readily accessible to MB^+. It is well known that the contact of iron with water yields massive oxidation which results in the formation of aggregates of iron nanoparticles with their surfaces rich in oxides and oxohydroxides. The surface of iron is very dynamic in terms of chemical speciation and may contain amphoteric surface groups. The same solid can undergo various speciation in different solutions, causing the measured point of zero charge (PZC) values to vary widely. PZC values as low as 3.6 ± 0.7 were determined for hydroxide/oxohydroxide precipitates using a mass potentiometric titration method and a salt titration method [25]. For copper oxide, PZC was reported to occur around pH of 6.0 [26]. Nevertheless, the electrostatic approach does not eliminate the possibility of chemical complexation of the cationic dye with the oxide, hydroxide, and/or oxohydroxide groups on the nanoparticle surfaces. The effect of pH on dye removal by bimetallic nanoparticles is an area which seems open to further investigations.
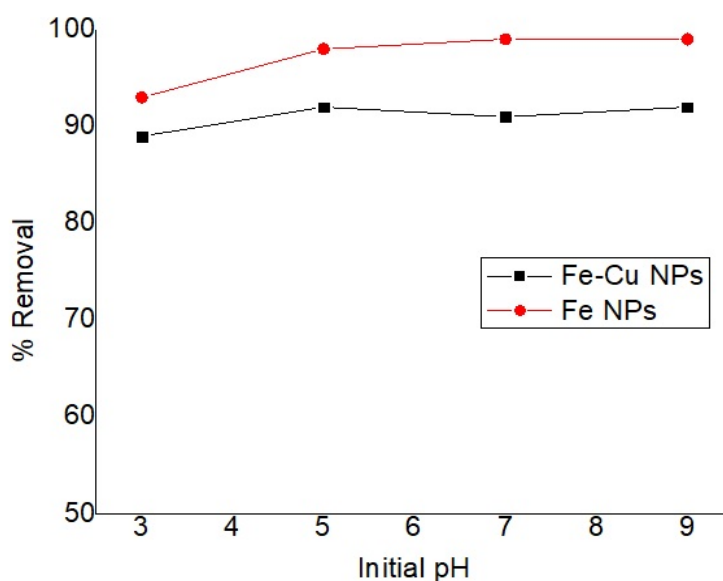
Figure 8: Variation of the percent removal of MB with different initial pH values using Fe NPs and Fe-Cu NPs.

3.2.4 Effect of Temperature

The effect of temperature was studied at two initial concentrations, and the results are provided in Table 3. The equilibrium concentrations of the dye in the phases were used to calculate the corresponding distribution constant, R_d, values, defined as:

$$R_d = (\frac{Q_e}{C_e})(\frac{m}{v})$$

Where Q_e (mg/g) stands for the mass of MB removed per g of the nanoparticle material, C_e (mg/L) is the equilibrium concentration of MB in solution, m (g) is the mass of the nanoparticle material, and v is the volume of solution (L). In this way, R_d becomes unit less, and can subsequently be used, as an empirical equilibrium constant, in the calculation of the enthalpy change of sorption:

$$\ln\left(\frac{R_{d2}}{R_{d1}}\right) = -\frac{\Delta H^0}{R}(\frac{1}{T_2} - \frac{1}{T_1})$$

Table 3: The obtained distribution constants and enthalpy changes for the removal of MB by Fe NPs and Fe-Cu NPs at two different initial concentrations.
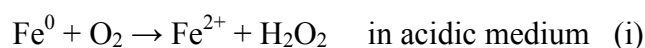
NPs	Initial Conc. (mg/L)	C_e (298K)	C_e (323K)	Q_e (298K)	Q_e (323K)	R_d (298K)	R_d (323K)	ΔH^0 (kJ/mol)
Fe	80.0	4.0	12.6	38.0	33.7	19.0	5.3	-40.6
Fe-Cu	80.0	13.6	19.0	33.2	30.5	4.9	3.2	-13.3
Fe	100.0	2.1	13.9	49.0	43.1	46.8	6.2	-64.8
Fe-Cu	100.0	16.5	31.5	41.8	34.3	5.1	2.2	-27.0

The obtained ΔH^0 values indicate that the sorption process is exothermic in both cases. MB exist in aqueous solution as hydrated cationic molecules $[MB(H_2O)_n]^+$ [27], and the observed exothermic behavior suggests that the dehydration process of the cationic entities costs less energy than the energy

liberated as a result of the intrinsic adsorption step, such that the overall energy change is negative. The obtained values of enthalpy change in the case of MB removal by Fe NPs clearly exceeds that of Fe-Cu NPs. This is not necessarily a consequence of the bond energies in the two cases, and can be linked as well to the variation in the dehydration energies of hydrated MB^+ cations in the two sorption systems.

3.2.5 Application of Fe NPs and Fe-Cu NPs as Heterogeneous Fenton Catalysts
In addition to their application in the removal of aqueous pollutants by redox and sorption mechanisms, Fe NPs have been used as a source of Fe^{2+} ions in heterogeneous Fenton reactions [e.g. 5,8,14,28]. The Fenton cycle in this case operates in a different way than the traditional one, and can be represented by the following reactions [8]:

$$Fe^0 + O_2 \rightarrow Fe^{2+} + H_2O_2 \quad \text{in acidic medium} \quad \text{(i)}$$

$$Fe^0 + H_2O_2 \rightarrow Fe^{2+} + 2H_2O_2 \quad \text{(ii)}$$

$$Fe^{2+} + H_2O_2 \rightarrow Fe^{3+} + OH\cdot + OH^- \quad \text{(iii)}$$

In this preliminary assessment, Fe NPs and Fe-Cu NPs have been tested as heterogeneous Fenton catalysts. The percent removal of the dye is shown in Fig. 9. For the sake of comparison, the figure contains the percent removal when the materials are used as heterogeneous Fenton catalysts, and when they are directly used as sorbents.

While Fe NPs behave almost in the same way in both cases, the results indicate that the performance of Fe-Cu bimetallic NPs is clearly enhanced when used as a heterogeneous catalyst, and the removal of the dye is almost complete (99.6%), and exceeds that of Fe NPs (98.0%). This agrees with previous results suggesting that Fe-containing bimetallic nanoparticles are more active than Fe NPs as heterogeneous Fenton catalysts [8]. Compared with Fe NPs, the Fe-Cu bimetallic nanoparticles seem to be experiencing different surface dynamics, leading to better capability of electron supply needed to catalyze the Fenton cycle. The topic seems open to further investigation.
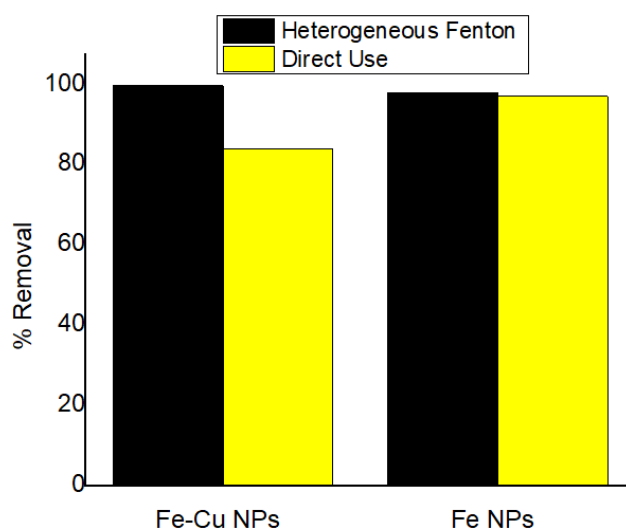
Figure 9. Percent removal of MB upon using the nanoparticle materials as heterogeneous Fenton catalysts, and as sorbents.

Conclusion

Fe NPs and Fe-Cu NPs were synthesized by liquid-phase reduction method. The particle size of the bimetallic nanoparticles was smaller than that of Fe NPs. The extent of dye removal of Fe NPs was higher than that of Fe-Cu NPs. The removal of MB dye on both nanomaterials can be described with Freundlich isotherm. At higher pH values, higher extents of dye removal were observed. According to preliminary results, Fe-Cu NPs showed better performance when used as heterogeneous Fenton catalysts. The application of the bimetallic nanoparticle materials as heterogeneous Fenton catalysts is open to further investigations.

References

1. E. Lefevre, N. Bossa, M.R. Wiesner, C.K. Gunsch, A review of the environmental implications of in situ remediation by nanoscale zero valent iron (nZVI): Behavior, transport and impacts on microbial communities, *Sci. Total Environ.* 565 (2016) 889-901.
2. S. Li, W. Wang, F. Liang, W-x. Zhang, Heavy metal removal using nanoscale zero-valent iron (nZVI): Theory and application, *J. Hazard. Mater.* 322 (2017) 163-171.
3. B.D. Yirsaw, M. Megharaj, Z. Chen, R. Naidu, Environmental application and ecological significance of nano-zero valent iron, *J. Environ. Sci.* 44 (2016) 88-98.
4. C. D. Raman, S. Kanmani, Textile dye degradation using nano zero valent iron: A review, *J. Environ. Manage.* 177 (2016) 341-355.
5. T. Shahwan, S. Abu Sirriah, M. Nairat, E. Boyacı, A.E. Eroğlu, T.B. Scott, K.R. Hallam, Green synthesis of iron nanoparticles and their application as a Fenton-like catalyst for the degradation of aqueous cationic and anionic dyes, *Chem. Eng. J.* 172 (2011) 258-266.
6. N. Efecan, T. Shahwan, A.E. Eroğlu, I. Lieberwirth, Characterization of the uptake of aqueous Ni^{2+} ions on nanoparticles of zero-valent iron (nZVI), *Desalination* 249 (2009) 1048-1054.
7. T. Phenrat, N. Saleh, K. Sirk, R.D. Tilton, G.V. Lowry, Aggregation and sedimentation of aqueous nanoscale zerovalent iron dispersions, *Environ. Sci. Technol.* 41 (2007) 284–290.
8. W.-J. Liu, T.-T. Qian, H. Jiang, Bimetallic Fe nanoparticles: Recent advances in synthesis and application in catalytic elimination of environmental pollutants, *Chem. Eng. J.* 236 (2014) 448-463.
9. M.F. Ourique, P.V.F. Sousa, A.F. Oliveira, R.P. Lopes, Comparative study of the direct black removal by Fe, Cu, and Fe/Cu nanoparticles, *Environ. Sci. Pollut. Res.* 25 (2018) 28928–28941.
10. T. Sun, M. Gong, Y. Cai, S. Xiao, L. Zhang, Y. Zhang, Z. Xu, D. Zhang, Y. Liu, C. Zhou, MCM-41-supported Fe(Mn)/Cu bimetallic heterogeneous catalysis for enhanced and recyclable photo-Fenton degradation of methylene blue, *Res. Chem. Intermed.* 46 (2020) 459–474.
11. S.A. Hashemizadeh, M. Biglari, Cu:Ni bimetallic nanoparticles: facile synthesis, characterization and its application in photodegradation of organic dyes, *J. Mater. Sci.: Mater. Electron.* 29 (2018) 13025–13031.
12. T.B. Nguyen, C.D. Dong, C.P. Huang, C.-W. Chen, S.-L. Hsieh, S. Hsieh, Fe-Cu bimetallic catalyst for the degradation of hazardous organic chemicals exemplified by methylene blue in Fenton-like reaction, *J. Environ. Chem. Eng.* 8 (2020) 104139.

13. L. Sun, H. Song, Q. Li, A. Li, Fe/Cu bimetallic catalysis for reductive degradation of nitrobenzene under oxic conditions, *Chem. Eng. J.* 283 (2016) 366-374.
14. K. Choi, W. Lee, Enhanced degradation of trichloroethylene in nano-scale zero-valent iron Fenton system with Cu(II), *J. Hazard. Mater.* 211–212 (2012) 146-153.
15. R. Sawafta, T. Shahwan, A Comparative study of the removal of methylene blue by iron nanoparticles from water and water-ethanol solutions, *J. Mol. Liq.* 273 (2019) 274-281.
16. A. Hamdy, M.K. Mostafa, M. Nasr, Zero-valent iron nanoparticles for methylene blue removal from aqueous solutions and textile wastewater treatment with cost estimation, *Water Sci. Technol.* 78 (2018) 367–378.
17. K. Sarmah, S. Pratihar, Synthesis, characterization, and photocatalytic application of iron oxalate capped Fe, Fe–Cu, Fe–Co, and Fe–Mn oxide nanomaterial, *ACS Sustainable Chem. Eng.* 5 (2017) 310–324.
18. M. Nairat, T. Shahwan, A.E. Eroglu, H. Fuchs, H., Incorporation of iron nanoparticles into clinoptilolite and its application for the removal of cationic and anionic dyes, *J. Ind. Eng. Chem.* 21 (2015) 1143–1151.
19. B. Schrick, J.L. Blough, A.D. Jones, T.E. Mallouk, Hydrodechlorination of trichloroethylene to hydrocarbons using bimetallic nickel-iron nanoparticles, *Chem. Mater.* 14 (2002) 5140–5147.
20. R. Naser, T. Shahwan, Comparative assessment of the decolorization of aqueous bromophenol blue using Fe nanoparticles and Fe-Ni bimetallic nanoparticles, *Desalin. Water Treat.* 159 (2019) 346–355.
21. A. Liu, J. Liu, B. Panac, W-x. Zhang, Formation of lepidocrocite (γ-FeOOH) from oxidation of nanoscale zero-valent iron (nZVI) in oxygenated water, *RSC Adv.* 4 (2014) 57377-57382.
22. RRUFF database: http://rruff.info/ (last access date:16.11.2020).
23. A.P. Grosvenor, B.A. Kobe, M.C. Biesinger, N.S. McIntyre, Investigation of multiplet splitting of Fe 2p XPS spectra and bonding in iron compounds, *Surf. Interface Anal.* 36 (2004) 1564–1574.
24. M.C. Biesingera, L.W.M. Laua, A.R. Gersonb, R.S. Smart, Resolving surface chemical states in XPS analysis of first row transition metals, oxides and hydroxides: Sc, Ti, V, Cu and Zn, *Appl. Surf. Sci.* 257 (2010) 887–898.
25. A.M. Cardenas-Peña, J.G. Ibanez, R. Vasquez-Medrano, Determination of the point of zero charge for electrocoagulation precipitates from an iron anode, *Int. J. Electrochem. Sci.* 7 (2012) 6142 – 6153.
26. J.R. Conway, A.S. Adeleye, J. Gardea-Torresdey, A.A. Keller, Aggregation, dissolution, and transformation of copper nanoparticles in natural waters, *Environ. Sci. Technol.* 49 (2015) 2749–2756.
27. Z. Zhao, E. Malinowski, Determination of the hydration of methylene blue aggregates and their dissociation constants using visible spectroscopy, *Appl. Spectrosc.* 53 (1999) 1567-1574.
28. S. Zha, Y. Cheng, Y. Gao, Z. Chen, M. Megharaj, R. Naidu, Nanoscale zero-valent iron as a catalyst for heterogeneous Fenton oxidation of amoxicillin, *Chem. Eng. J.* 255 (2014) 141-148.

(2021) ; http://www.jmaterenvironsci.com